

Quantum dot nanophotonics – from waveguiding to integration

Lih Y. Lin,^{a,b} Chia-Jean Wang,^{a,c} Michael C. Hegg,^a and Ludan Huang^b

^a Department of Electrical Engineering, University of Washington, Seattle, WA 98195-2500, USA

lin@ee.washington.edu

^b Department of Physics, University of Washington, Seattle, WA 98195, USA

^c Currently with Intellectual Ventures, Bellevue, WA 98004, USA

Abstract. Due to its unique optoelectronic properties, the quantum dot (QD) has become a promising material for realizing photonic components and devices with high quantum efficiencies. Quantum dots in colloidal form can have their surfaces modified with various molecules, which enables new fabrication process utilizing molecular self-assembly and can result in new QD photonic device structures in nano-scale. In this review paper, we describe our work on QD waveguides for sub-diffraction limit waveguiding that utilizes near-field optical coupling between QDs, nano-scale QD photodetectors with nanogaps for sensing with high spatial resolution and sensitivity, as well as integration of these two nanophotonic components. The QD waveguide achieved a transmission loss of 3 dB/4 μm , which is lower than the experimental results from other sub-diffraction limit waveguides that have been reported. It also demonstrated a comparable waveguiding effect through a waveguide with a sharp bend. The QD photodetector showed a sensitivity of 60 pW over a device with a nanogap of 25 nm for detection. The compatibility between the fabrication processes for these two components with colloidal QDs allows integration of them through self-assembly fabrications.

Keywords: quantum dot, waveguide, photodetector, sub-diffraction limit, self-assembly, nanophotonics.

1 INTRODUCTION

The constant demand for smaller and faster computation and communication systems with versatile functionality has been driving the miniaturization, integration density and speed of device technologies. While electronics face challenges in speed, power consumption and crosstalk between information channels, photonics emerges as a promising alternative. Nevertheless, the development of photonic integrated circuits has been hindered by the diffraction limit, which constraints the integration density one can achieve using photons as information carrier.

Thanks to the advances in nano-fabrication technologies, nano-scale structures such as photonic crystals [1-3] and silicon slot waveguides [4-7] have been demonstrated to transmit optical wave with high confinement. One-dimensional nano-structures such as nanowires, nanotubes [8-10] and 0-dimensional structures such as semiconductor quantum dots (QD) and metal nanoparticles (NP) have also offered promising routes towards waveguiding in nano-scale. Among various technologies, transmitting optical energy as surface plasmon propagation can achieve true sub-diffraction waveguiding [11-15]. Plasmonic waveguide structures that have been proposed thus far include 1-D negative index optical fibers [16, 17], metal nanowires [18, 19], metal strips [20, 21], triangular metal wedges [22], metal slots [23-25] and metal NPs [26-31]. The chief challenge for plasmonic waveguides is the high transmission loss due to strong damping of the propagating surface plasmon. Integration of the plasmonic waveguides with active semiconductor devices such as lasers or photodetectors is also challenging. Recently, combination of dielectric waveguiding with surface plasmon

polariton (SPP) propagation was proposed, with confinement from the SPP propagation as a trade-off with low-propagation loss from the dielectric waveguiding [32].

Semiconductor QDs, on the other hand, are gain-enabled materials under excitation. They have spectrally sharp emission peaks and high quantum efficiency due to their 3-D electron-hole pair (exciton wavefunction) confinement. Their spectral response can easily be tuned by particle size and composition. These properties make QDs ideal materials for optoelectronic applications [33]. Conventional QD photonic devices utilize self-organization at the interface of strained epitaxially grown III-V or II-VI semiconductor layers to create QD nanostructures. Such process is often not compatible with silicon CMOS fabrication. Another process to fabricate QDs is through chemical synthesis. The resulting QDs are in colloidal form and have been widely used as fluorescent tags in biomedicine [34]. Colloidal QDs conjugated with streptavidin or carboxylated QDs can be fabricated into a waveguide pattern on a silicon wafer through DNA-mediated [35] or other molecular self-assembly processes [36]. Utilizing the optical gain within and near-field optical coupling between the QDs, sub-diffraction optical energy transmission with low loss using such devices has been proposed [35, 37-40].

As the integration density of photonic integrated circuits progresses towards the sub-micron regime, it becomes imperative to detect the optical signal with nanometer resolution as well in order to preserve the on-chip integration density. The requisite photodetection devices are critical for integration of nanophotonics with electronics. Previous approaches to near-field optical detection using nanostructures include single [41] and crossed-nanowire [42] devices, photosensitive carbon nanotubes [43], single-electron-transistors (SETs) [44, 45], optical-antenna structures [46], and nanocrystal-enhanced photonic crystal structures [47]. These novel approaches, while advancing certain aspects of nanoscale photodetection, either do not provide the fabrication flexibility and convenient materials necessary for nanophotonic integrated circuit design or have large overall device sizes. With their unique optoelectronic property and surface chemistry, colloidal QDs incorporated into nanostructures are promising candidates for photodetection in nanophotonic integrated circuits. Furthermore, carrier multiplication has been shown to be highly efficient in colloidal QDs due to confinement-enhanced Coulomb coupling between single- and multi-exciton states, which is a unique feature of semiconductor nanocrystals [48]. Internal quantum efficiencies as high as 700% have been experimentally demonstrated [49], suggesting the possibility for ultra-high sensitivity photodetection using this material. Utilizing these unique properties of colloidal QDs, nanoscale QD photodetectors with high sensitivity (< 60 pW) have been fabricated and demonstrated [50]. Integrated fabrication of such photodetector with the QD waveguides is also straightforward through self-assembly fabrication [51]. The fabrication processes of individual QD components and integration can be performed on a variety of substrates with proper surface coating, which adds additional strength to QD nanophotonics.

In this paper, we review our previous works on QD waveguides, photodetectors, as well as integration of these two components via self-assembly approach.

2 SUB-DIFFRACTION LIMIT QD WAVEGUIDE

Our approach combines ‘bottom-up’ self-assembly of colloidal QDs with ‘top-down’ lithography on a silicon chip to build nanophotonic components and systems. Based on near-field interaction between photo-excited QDs, sub-diffraction optical waveguides can be built. We have demonstrated efficient sub-diffraction limit waveguiding in self-assembled CdSe/ZnS core/shell QD arrays including 90° bends [38, 39]. By taking advantage of the versatility of chemical functionalization of both the substrate as well as the QDs, through molecular recognition, the QDs can be precisely arranged into desired locations defined lithographically [35, 52, 53]. For example, 3’aminopropyltriethoxysilane (APTES) is an efficient linker molecule between carboxylated QDs and a Si/SiO₂ substrate. Alternatively, a

chain of molecules including 3-mercaptopropyltrimethoxysilane (MPTMS), acrylamide modified single-stranded DNA (ss-DNA) in series can bind streptavidin QDs linked to biotinylated complementary DNA (cDNA) to achieve self-assembly with programmability [38].

Shown in Fig. 1(a) is the principle of the QD waveguide. The surface-anchored closely spaced QDs in the waveguide are excited by a continuous-wave pump laser into the lowest exciton state. The input signal stimulates the emission of the QD which will then cascade through the waveguide. Finite difference time domain (FDTD) simulation indicates that the intensity distribution of the stimulated emitted photons is highly concentrated around the QD and attenuates rapidly, as shown in Fig. 1(b). Due to the strong near-field inter-dot coupling and optical gain in each QD, low-loss transmission with low crosstalk can be achieved [35, 37].

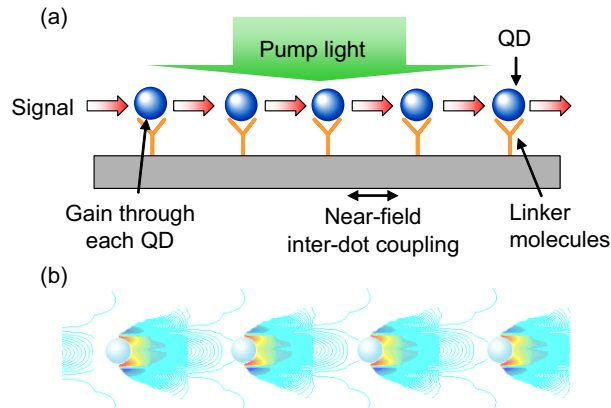


Fig. 1. (a) Schematic drawing of the sub-diffraction QD waveguide. (b) Intensity distribution of the stimulated emitted photons by FDTD simulation.

Self-assembly fabrication of the QD waveguide through the mediation of APTES is shown here as an example. The fabrication process, shown in Fig. 2, starts with oxygen plasma treatment of a silicon wafer coated with silicon dioxide at 20 W for 60 seconds following electron-beam lithography (EBL) of the waveguide pattern. Then, the sample is immersed into 0.1~0.2% v/v APTES thoroughly mixed in a 95% IPA and 5% DI H₂O solvent; for instance, 4 μ L APTES would be mixed in 1900 μ L IPA and 100 μ L DI to make 0.2% solution. After 1 minute reaction time, the sample is removed and rinsed in IPA. The chemisorption of APTES leads to an amine (-NH₂) group presented at the terminal. Afterwards, the sample is placed on a hot plate for 7.5 minutes at 110°C to cure the monolayer [54]. Attachment of QDs is achieved by depositing a droplet of 0.125 μ M carboxylated QDs mixed in DI H₂O with 1 mM 1-ethyl-3-(3'-dimethylaminopropyl)-carbodiimide (EDC), a coupling reagent that aids in binding amine and carboxyl groups directly on the patterned region. After one hour wait time, the QD solution is rinsed off the substrate with 1x phosphate buffer solution followed by 0.3 M ammonium acetate to remove the salts from the buffer. The sample is then blown dry with N₂. For the final steps, the PMMA is dissolved with dichloromethane, CH₂Cl₂, via a three minute immersion process [55], and the sample is rinsed with DI H₂O and again dried under a nitrogen stream.

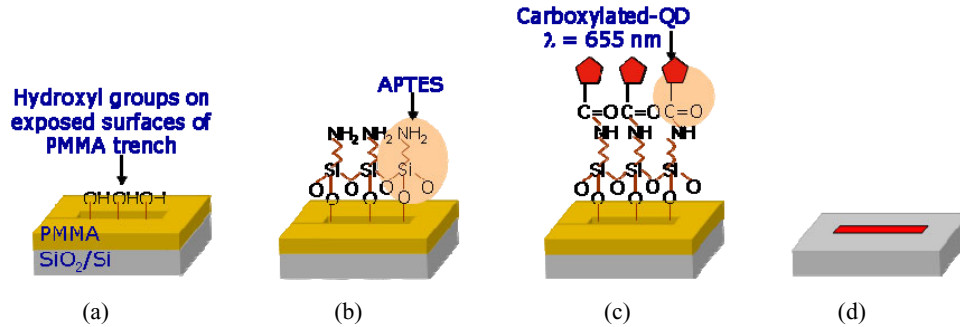


Fig. 2. QD waveguide self-assembly fabrication through APTES: (a) EBL pattern a SiO₂/Si sample coated with PMMA; develop PMMA; treat with oxygen plasma to create hydroxyl groups on surface; (b) Solution phase deposition of APTES; (c) Carboxylated QDs covalently bind to the amine groups of APTES; (d) Strip PMMA to leave waveguide. [38]

Figure 3 shows fluorescence and AFM images of the fabricated QD waveguide in 500-nm and 100-nm width. The fluorescence shows spontaneous emission of the QDs, while the AFM images indicate the distribution and coverage of the QDs in the waveguide structure. In our experiments, a 2-D array of QDs is built by self-assembly on a prestructured substrates patterned by EBL with finite width. As discussed in Ref. [40], this does not compromise the performance of the QD waveguide. Rather, reduced transmission can be facilitated through cross-coupling.

We have demonstrated efficient optical signal transport in QD waveguides even with corners and bends [38]. With a 405-nm pump laser focused on the waveguide through a 20x objective lens and a 639-nm signal laser coupled to the waveguide through a tapered fiber, we measured the transmitted optical signal through the QD waveguide and compared the result to direct coupling between input and output fibers spaced at the same distance. The experimental results, shown in Fig. 4, indicate the waveguiding effect with the QD waveguide. Both a straight waveguide 20- μ m in length and a waveguide of the same length but with 90° bend in the middle achieve similar performance. This shows the potential of flexible routing for ultra-high density photonic integrated circuits using the QD waveguide.

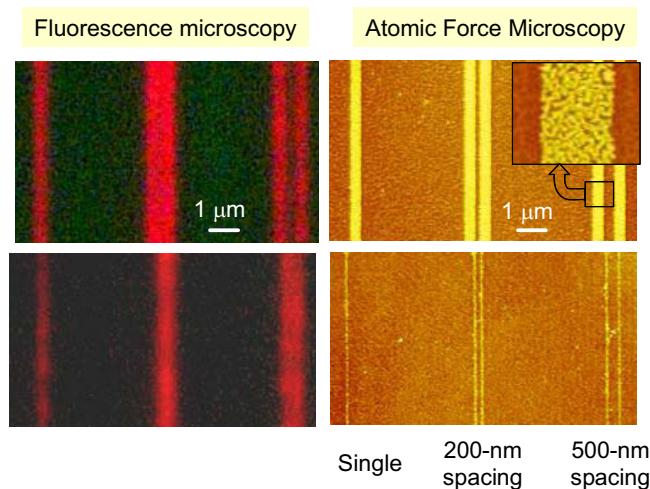


Fig. 3. QD waveguides with 500-nm (top) and 100-nm (bottom) width in single and pair formations spaced 200 nm and 500 nm apart. The fluorescence image shows far-field emission. The AFM image shows details of the waveguides where individual QDs can be seen.

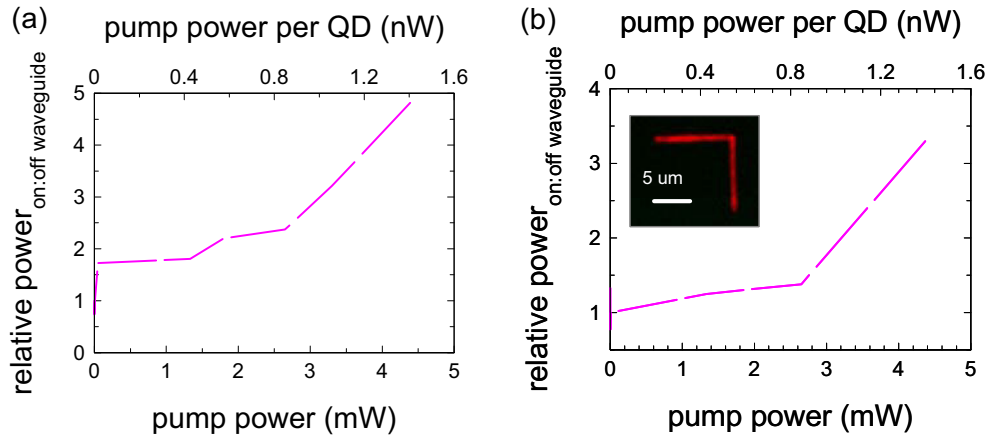


Fig. 4. Ratio of the transmitted power through the QD waveguide to that through direct coupling for (a) a straight waveguide 20 μm in length; (b) a waveguide of the same length with 90° bend in the middle.

The transmission loss per unit length of the QD waveguide was characterized by measuring the output signal across multiple lengths ranging from 4 μm to 10 μm . Waveguides with 500 nm (Fig. 5a) and 100 nm (Fig. 5b) widths were examined. Varying the pump power per QD from 1.18 nW to 2.08 nW produced the same upward trend in transmission at higher optical intensities. Additionally, the narrow waveguides revealed steeper slopes. Subsequently, we use an exponential fit to the data since the output power follows the relation, $P(z) = P_0 \exp(-\alpha z)$, with respect to the input power P_0 and the loss coefficient, α . As a result, we can extract an average loss value of 3 dB per 2.26 μm and 4.06 μm for the 100 nm and 500 nm width waveguides across the three pump settings. The trend of lower loss for wider waveguide is consistent with Monte Carlo simulation of the QD waveguide transmission that takes into account of lateral cross-coupling between QDs [40].

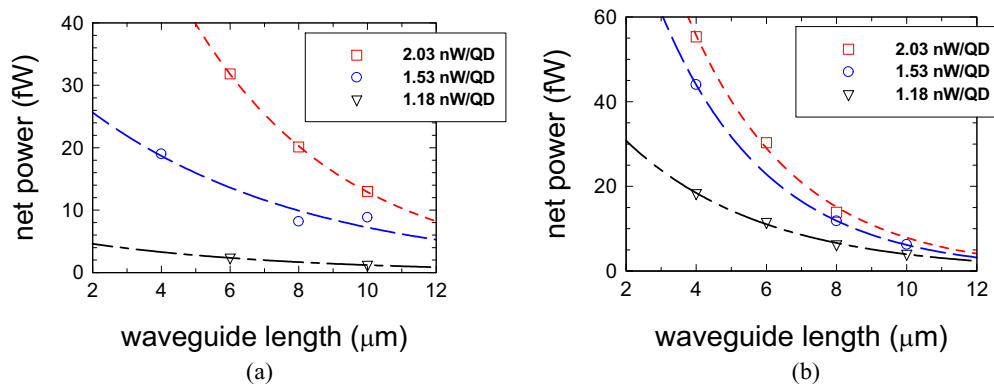


Fig. 5. QD waveguide loss behavior measured over multiple lengths and pump powers. (a) 500 nm wide QD waveguides. (b) 100 nm wide QD waveguides.

Table 1 compares the reported theoretical and experimental findings for all proposed true sub-diffraction waveguiding methods. Most of these rely on surface plasmon propagation except the QD waveguide. With the exception of the gold insulator-metal-insulator (IMI) junctions, the QD array waveguide has the best transmission loss figure measured

experimentally. The transmission loss can be further reduced by improving the self-assembly fabrication process to increase the coverage density of the QDs.

Table 1. A comparison of theoretical and experimental loss for sub-diffraction limit waveguiding methods.

<i>Method</i>	<i>Device dimensions</i>	<i>Wavelength</i>	<i>Theoretical loss</i>	<i>Experimental loss</i>
Ag pin 1D fiber [16]	20 nm diameter core	633 nm	7.31 dB/ μm = 3 dB/410 nm	N/A
Au nanowire [18]	200 nm width 50 nm thickness	800 nm	N/A	1.7 dB/ μm = 3 dB/1.76 μm
Ag wedge [22]	300 nm base 40° angle	632 nm	1.9 dB/ μm = 3 dB/1.58 μm	2.9 dB/ μm = 3 dB/1.03 μm
Ag nanoparticle array [31]	50 nm diameter 25 nm inter-dot separation	488 nm	4.8 dB/ μm = 3 dB/614 nm	N/A
Ag nanoparticle array [12]	50 nm diameter 50 nm inter-dot separation	570 nm	30 dB/ μm = 3 dB/100 nm	31 dB/ μm = 3 dB/97 nm
Au IMI [13]	2D coverage 45 nm thickness	1.55 μm	0.00076 dB/ μm = 3 dB/3.9 mm	N/A
Au IMI in Si [23]	150 nm width 250 nm thickness	1.55 μm	0.55 dB/ μm = 3 dB/5.45 μm	0.8 dB/ μm = 3 dB/3.75 μm
Au clad MIM [56]	150 nm width 100 nm thickness	633 nm	12.2 dB/ μm = 3 dB/246 nm	N/A
Au clad index-guided MIM [56]	150 nm width 100 nm thickness	633 nm	3.1 dB/ μm = 3 dB/968 nm	N/A
QD waveguide	500 nm width 100 nm width	639 nm	N/A	3 dB/4.06 μm 3 dB/2.26 μm

3 NANOSCALE QD PHOTODETECTOR

A nanoscale QD photodetector that can easily be integrated with the QD waveguide is shown in Fig. 6. Colloidal QDs are placed between two electrodes spaced with a nano-gap, so that electrons can tunnel between the electrodes through the QDs. Electron transport in colloidal QDs embedded in an n-i-n (metal-QD-metal) structure typically involves significant potential barriers at the QD-QD interface as well as the QD-electrode interface. Transport between QDs can, therefore, be considered as a problem of hopping between localized states [57], and can be modeled by the transfer Hamiltonian approach [58]. Carriers with higher energies have a higher probability of tunneling through the QDs and contributing to the tunneling current. The effect of optical excitation on the electrical transport of such structures is thus to reduce the effective potential barrier from the QD to the electrode by exciting photo-generated carriers into higher energy states. The tunneling current increases when the QDs are photo-excited, thus achieving photodetection.

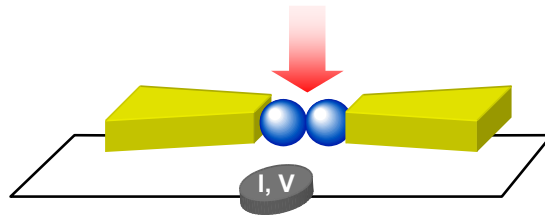


Fig. 6. Schematic drawing of the nanoscale QD photodetector. The photo-excitation of the QDs in the junction will modulate a tunneling current.

Fabrication of the nano-gap electrodes can be performed using break-junction process that involves electromigration of the Au atoms [59]. Electrodes having widths of 50 nm have been broken with controlled gap sizes ranging from 1.5 - 25 nm. Figure 7(a) shows a large-area device structure and the magnified nano-gap region, with a 25-nm gap obtained through the break-junction process. Alternatively, high-resolution EBL can also be used to pattern the nano-gap electrodes in parallel and eliminate the break-junction step, which is inherently a serial process. This will be described later in Sec. 4 [51]. After confirmation of the break using SEM, a 100 μ M solution of CdSe/ZnS core/shell QDs in toluene is drop-cast onto the wafer. The QDs have a nominal diameter of 5.2 nm and an emission wavelength of 620 nm. Figure 7(b) shows an example of a device after drop-casting NCQDs into the nano-gap. [50]

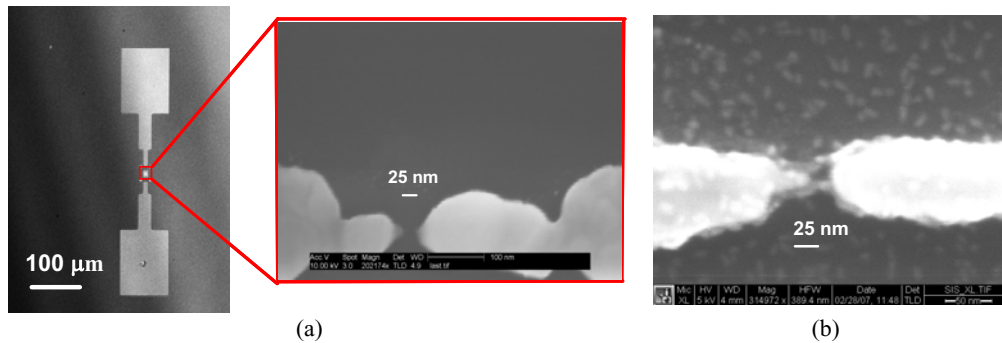


Fig. 7. SEM images of (a) a pre-QD deposition break-junction electrode, and (b) a nano-scale QD photodetector after QD deposition.

The drop-cast deposition method results in a thin film of QDs over a large area, but only QDs in and around the nano-gap can contribute significantly to the measured current, thus achieving high spatial resolution. To determine the effective area of the photodetector, we used finite element modeling to simulate the electric field intensity in and around the nanogap. Figure 8(a) shows a surface plot of the E-field intensity for a 20 nm nano-gap device. The E-field is highest around the edges of the gap and decreases radially outward from the center, as shown in Fig. 8(b). For this device, E/E_{\max} is approximately 10% when $r = 50$ nm. An effective area of the device is defined as the rectangular area of the nano-gap plus a circular area with radius r defined by the distance from the electrode edge at which the E-field is 10% of the highest value [50]. This distance scales linearly with gap size.

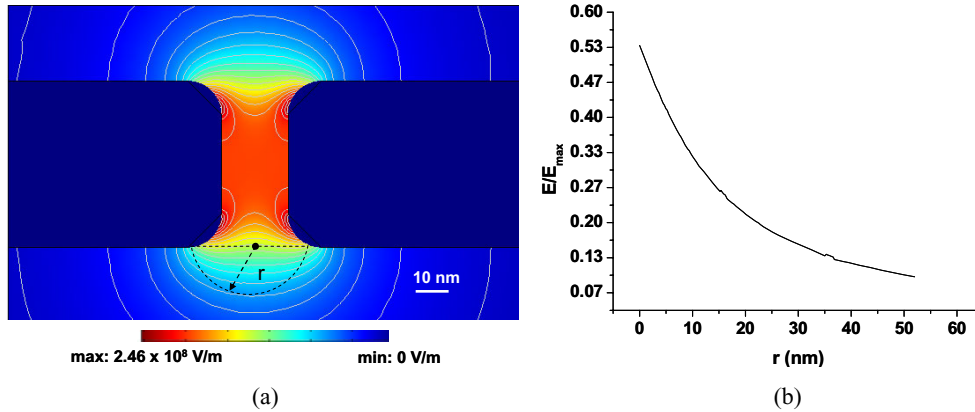


Fig. 8. (a) Finite element simulation of the electric field intensity in and around a 20 nm nano-gap. (b) E/E_{\max} vs. radial distance from the electrode edge.

Figure 9 shows the I-V characteristics of a 25-nm gap device under illumination and dark conditions. The illumination intensity is 1 pW/nm^2 . The sensitivity and responsivity of the device was then characterized by measuring photocurrent under various illumination intensities with the device biased at 4 V. A Keithley 6430 Sub-Femtoamp source meter and a Cascade Microtech M150 low-noise probe station are used for the measurements. The results are shown in Fig. 10. The device starts to show measurable photocurrent of 80 fA under 60 pW illumination over the effective device area. No special shielding of ambient light was done for this measurement. The device has an average responsivity of 2.7 mA/W under low-intensity illumination, and starts to exhibit saturation effects when the optical power increases beyond 4 nW.

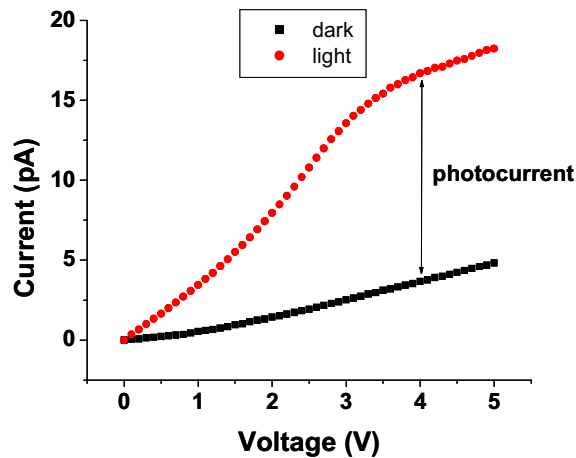


Fig. 9. I-V characteristics of the QD photodetector under dark (squares) and illuminated (circles) conditions.

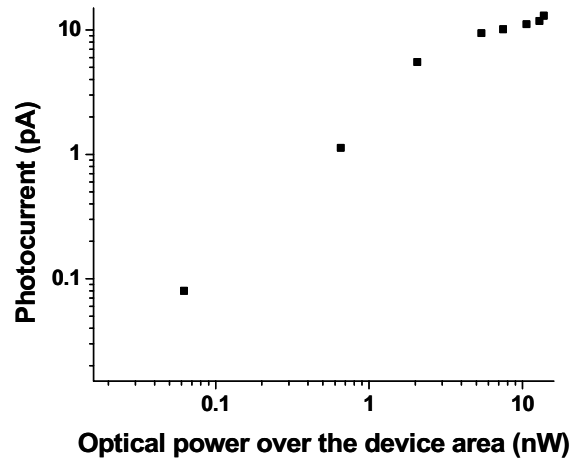


Fig. 10. Measured photocurrent versus input laser power for the QD photodetector. The device is biased at 4V and the wavelength of the incident laser is 405 nm.

The QD photodetector described here is not likely to outperform conventional photodetectors in terms of responsivity due to its small active volume. However, the main advantage of the nanoscale QD photodetector lies in its high sensitivity, small size and spatial resolution, which allows integration with sub-diffraction optical waveguides that are closely spaced without compromising the integration density of the waveguides and the overall nanophotonic integrated circuits. The QD photodetector is fabricated upon a silicon substrate and does not require epitaxial growth of the material, which makes integration with other nanophotonic waveguides such as nanowires, plasmonic materials, photonic crystals, or high-index silicon-on-insulator devices readily achievable.

4 INTEGRATION OF QD DEVICES

Fabrication of the QD waveguide/photodetector integrated device is achieved by multiple alignment-assisted EBL patterning of the QD waveguide, nanogap electrodes, and self-assembled QD deposition. To minimize the effect of processing on QDs and the linker molecules for self-assembly, we start with EBL patterning and Au evaporation of the nanogap electrodes. It is found that a gap size of 10 to 30 nm can be consistently achieved by writing at 30 kV, 15.0 pA current and a dose of 0.5-0.6 nC/cm with the EBL apparatus in use (FEI Sirion SEM). As can be seen from the SEM images shown in Fig. 11, the EBL-patterned nano-gaps exhibit more abrupt edges and a cleaner break than those by electromigration-induced break-junction technique (shown in Fig. 7). For the integrated device, EBL nano-gap patterning also simplifies the process because it creates both the electrodes and nano-gaps in one EBL writing, while the electro-migration induced break junction process requires an additional step of breaking the junctions in series. Furthermore, EBL patterning provides more consistent control over the nano-gap size through lithography than the electromigration-induced break-junction technique, especially in the range of 10-30 nm.

After characterizing the size and position of the nano-gaps using an SEM, a second EBL is performed to define the waveguide pattern, which is aligned to the nano-gap. We then perform the self-assembly fabrication steps for the QD waveguides. For the molecular self-assembly process, the Si/SiO₂ wafer is oxygen-plasma treated to create -OH groups on the exposed SiO₂ surface and APTES is deposited by immersing the sample in solution to create a surface expressing amines for further chemical reaction [53]. A droplet of carboxylated QDs suspended in 1x phosphate buffer solution (PBS) mixed with 1-ethyl-3-(3-

dimethylaminopropyl)-carbodiimide (EDC), an amine-carboxyl coupling reagent, is applied to the sample as the second layer. After waiting for a minimum of one hour during which the QDs bind to the sample, excess material is rinsed off with 1x PBS buffer and the PMMA is also removed with dichloromethane to reveal the waveguides. As an example, Fig. 11 shows the SEM image of a QD photodetector with 12-nm gap integrated with a 52 nm-wide QD waveguide [51].

In this first demonstration of QD waveguide and photodetector integrated device, we have used the same QDs for the waveguide and the photodetector. To optimize the performance of the integrated device, nanocrystal with different sizes can be chosen so that the emission peak of the waveguide QDs overlaps the absorption peak of the photodetector QDs. Deposition of multiple quantum dot types can be achieved by introducing an additional EBL patterning to pattern the waveguide and nano-gap area separately.

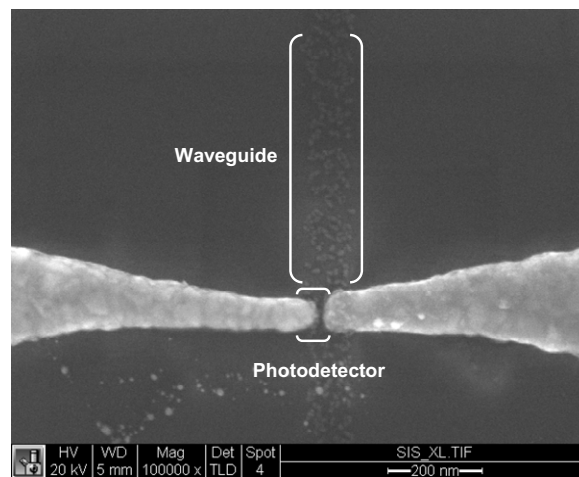


Fig. 11. SEM image of a 52-nm wide QD waveguide integrated with a QD photodetector with 12-nm gap.

Acknowledgments

C.-J. Wang would like to thank the NSF Graduate Fellowship Program and the Intel Fellowship for financial support. M. C. Hegg thanks the NSF IGERT Graduate Fellowship Program and University of Washington UIF Graduate Fellowship Program for financial support. This work was performed in part at the University of Washington Nanotech User Facility (NTUF), a member of the National Nanotechnology Infrastructure Network (NNIN), which is supported by the National Science Foundation.

References

- [1] S. G. Johnson, P. R. Villeneuve, S. Fan, and J. D. Joannopoulos, "Linear waveguides in photonic-crystal slabs," *Phys. Rev. B* **62**, 8212-8222 (2000) [[doi:10.1103/PhysRevB.62.8212](https://doi.org/10.1103/PhysRevB.62.8212)].
- [2] M. F. Yanik, S. Fan, M. Soljacic, and J. D. Joannopoulos, "All-optical transistor action with bistable switching in a photonic crystal cross-waveguide geometry," *Opt. Lett.* **28**, 2506-2508 (2003) [[doi:10.1364/OL.28.002506](https://doi.org/10.1364/OL.28.002506)].

- [3] E. Yablonovitch, "Photonic bandgap based designs for nano-photonic integrated circuits," *Tech. Dig. 2003 Int. Semicond. Dev. Res. Symp.*, 17-20 (2003) [doi:10.1109/ISDRS.2003.1272105].
- [4] W. Bogaerts, R. Baets, P. Dumon, V. Wiaux, S. Beckx, D. Taillaert, B. Luyssaert, J. Van Campenhout, P. Bienstman, and D. Van Thourhout, "Nanophotonic waveguides in silicon-on-insulator fabricated with CMOS technology," *J. Lightwave Technol.* **23**, 401-412 (2005) [doi:10.1109/JLT.2004.834471].
- [5] C. A. Barrios, V. R. Almeida, R. Panepucci, and M. Lipson, "Electrooptic modulation of silicon-on-insulator submicrometer-size waveguide devices," *J. Lightwave Technol.* **21**, 2332-2339 (2003) [doi:10.1109/JLT.2003.818167].
- [6] M. Lipson, "Overcoming the limitations of microelectronics using Si nanophotonics: Solving the coupling, modulation and switching challenges," *Nanotechnology* **15**, S622-S627 (2004) [doi:10.1088/0957-4484/15/10/020].
- [7] Q. Xu, V. R. Almeida, R. Panepucci, and M. Lipson, "Experimental demonstration of guiding and confining light in nanometer-size low-refractive index material," *Opt. Lett.* **29**, 1626-1628 (2004) [doi:10.1364/OL.29.001626].
- [8] C. J. Barrelet, A. B. Greytak, and C. M. Lieber, "Nanowire photonic circuit elements," *Nano Lett.* **4**, 1981-1985 (2004) [doi:10.1021/nl048739k].
- [9] M. Law, J. Goldberger, and P. Yang, "Semiconductor nanowires and nanotubes," *Annu. Rev. Mater. Res.* **34**, 83-122 (2004) [doi:10.1146/annurev.matsci.34.040203.112300].
- [10] M. Law, D. J. Sirbully, J. C. Johnson, J. Goldberger, R. J. Saykally, and P. Yang, "Nanoribbon waveguides for subwavelength photonics integration," *Science* **305**, 1269-1273 (2004) [doi:10.1126/science.1100999].
- [11] S. Lal, S. Link, and N. J. Halas, "Nano-optics from sensing to waveguiding," *Nature Photon.* **1**, 641-648 (2007) [doi:10.1038/nphoton.2007.223].
- [12] S. Maier, "Plasmonics: Metal nanostructures for subwavelength photonic devices," *IEEE J. Sel. Top. Quantum Electron.* **12**, 1214-1220 (2006) [doi:10.1109/JSTQE.2006.879582].
- [13] R. Zia, M. D. Selker, P. B. Catrysse, and M. L. Brongersma, "Geometries and materials for subwavelength surface plasmon modes," *J. Opt. Soc. Am. A* **21**, 2442-2446 (2004) [doi:10.1364/JOSAA.21.002442].
- [14] W. L. Barnes, A. Dereux, and T. W. Ebbesen, "Surface plasmon subwavelength optics," *Nature* **424**, 824-830 (2003) [doi:10.1038/nature01937].
- [15] S. I. Bozhevolnyi, V. S. Volkov, E. Devaux, J.-Y. Laluet, and T. W. Ebbesen, "Channel plasmon subwavelength waveguide components including interferometers and ring resonators," *Nature* **440**, 508-511 (2006) [doi:10.1038/nature04594].
- [16] J. Takahara, S. Yamagishi, H. Taki, A. Morimoto, and T. Kobayashi, "Guiding of a one-dimensional optical beam with nanometer diameter," *Opt. Lett.* **22**, 475-477, (1997).
- [17] J. Takahara and F. Kusunoki, "Guiding and nanofocusing of two-dimensional optical beam for nanooptical integrated circuits," *IEICE Trans. Electron.* **E90-C**, 87-94 (2007) [doi:10.1364/OL.22.000475].
- [18] J. R. Krenn, B. Lamprecht, H. Ditlbacher, G. Schider, M. Salerno, A. Leitner, and F. R. Aussenegg, "Non-diffraction-limited light transport by gold nanowires," *Europhys. Lett.* **60**, 663-669 (2002) [doi:10.1209/epl/i2002-00360-9].

- [19] R. M. Dickson and L. A. Lyon, "Unidirectional plasmon propagation in metallic nanowires," *J. Phys. Chem. B* **104**, 6095-6098 (2000) [[doi:10.1021/jp001435b](https://doi.org/10.1021/jp001435b)].
- [20] R. Zia, J. A. Schuller, and M. L. Brongersma, "Near-field characterization of guided polariton propagation and cutoff in surface plasmon waveguides," *Phys. Rev. B* **74**, 165415 (2006) [[doi:10.1103/PhysRevB.74.165415](https://doi.org/10.1103/PhysRevB.74.165415)].
- [21] L. Yin, V. K. Vlasko-Vlasov, J. Pearson, J. M. Hiller, J. Hua, U. Welp, D. E. Brown, and C. W. Kimball, "Subwavelength focusing and guiding of surface plasmons," *Nano Lett.* **5**, 1399-1402 (2005) [[doi:10.1021/nl050723m](https://doi.org/10.1021/nl050723m)].
- [22] D. F. P. Pile, T. Ogawa, D. K. Gramotnev, T. Okamoto, M. Haraguchi, M. Fukui, and S. Masuo, "Theoretical and experimental investigation of strongly localized plasmons on triangular metal wedges for subwavelength waveguiding," *Appl. Phys. Lett.* **87**, 061106 (2005) [[doi:10.1063/1.1991990](https://doi.org/10.1063/1.1991990)].
- [23] L. Chen, J. Shakya, and M. Lipson, "Subwavelength confinement in an integrated metal slot waveguide on silicon," *Opt. Lett.* **31**, 2133-2135 (2006) [[doi:10.1364/OL.31.002133](https://doi.org/10.1364/OL.31.002133)].
- [24] J. A. Dionne, L. A. Sweatlock, and H. A. Atwater, "Highly confined photon transport in subwavelength metallic slot waveguides," *Nano Lett.* **6**, 1928-1932 (2006) [[doi:10.1021/nl0610477](https://doi.org/10.1021/nl0610477)].
- [25] J. A. Dionne, L. A. Sweatlock, H. A. Atwater, and A. Polman, "Plasmon slot waveguides: Towards chip-scale propagation with subwavelength-scale localization," *Phys. Rev. B* **73**, 035407 (2006) [[doi:10.1103/PhysRevB.73.035407](https://doi.org/10.1103/PhysRevB.73.035407)].
- [26] M. L. Brongersma, J. W. Hartman, and H. A. Atwater, "Electromagnetic energy transfer and switching in nanoparticle chain arrays below the diffraction limit," *Phys. Rev. B* **62**, R16356-R16359 (2000) [[doi:10.1103/PhysRevB.62.R16356](https://doi.org/10.1103/PhysRevB.62.R16356)].
- [27] S. A. Maier, P. G. Kik, and H. A. Atwater, "Optical pulse propagation in metal nanoparticle chain waveguides," *Phys. Rev. B* **67**, 205402 (2003) [[doi:10.1103/PhysRevB.67.205402](https://doi.org/10.1103/PhysRevB.67.205402)].
- [28] S. A. Maier, P. G. Kik, H. A. Atwater, S. Meltzer, E. Harel, B. E. Koel, and A. A. G. Requicha, "Local detection of electromagnetic energy transport below the diffraction limit in metal nanoparticle plasmon waveguides," *Nature Mater.* **2**, 229-232 (2003) [[doi:10.1103/PhysRevB.67.205402](https://doi.org/10.1103/PhysRevB.67.205402)].
- [29] L. A. Sweatlock, S. A. Maier, H. A. Atwater, J. J. Penninkhof, and A. Polman, "Highly confined electromagnetic fields in arrays of strongly coupled Ag nanoparticles," *Phys. Rev. B* **71**, 235408 (2005) [[doi:10.1103/PhysRevB.71.235408](https://doi.org/10.1103/PhysRevB.71.235408)].
- [30] S. A. Maier, P. E. Barclay, T. J. Johnson, M. D. Friedman, and O. Painter, "Low-loss fiber accessible plasmon waveguide for planar energy guiding and sensing," *Appl. Phys. Lett.* **84**, 3990-3992 (2004) [[doi:10.1063/1.1753060](https://doi.org/10.1063/1.1753060)].
- [31] M. Quinten, A. Leitner, J. R. Krenn, and F. R. Aussenegg, "Electromagnetic energy transport via linear chains of silver nanoparticles," *Opt. Lett.* **23**, 1331-1333 (1998) [[doi:10.1364/OL.23.001331](https://doi.org/10.1364/OL.23.001331)].
- [32] R. F. Oulton, V. J. Sorger, D. A. Genov, D. F. Pile, and X. Zhang, "A hybrid plasmonic waveguide for subwavelength confinement and long-range propagation," *Nature Photon.* **2**, 496-500 (2008) [[doi:10.1038/nphoton.2008.131](https://doi.org/10.1038/nphoton.2008.131)].
- [33] V. I. Klimov, A. A. Mikhailovsky, S. Xu, A. Malko, J. A. Hollingsworth, C. A. Leatherdale, H.-J. Eisler, and M. G. Bawendi, "Optical gain and stimulated

- emission in nanocrystal quantum dots," *Science* **290**, 314-317 (2000) [[doi:10.1126/science.290.5490.314](https://doi.org/10.1126/science.290.5490.314)].
- [34] W. C. W. Chan and S. Nie, "Quantum dot bioconjugates for ultrasensitive nonisotopic detection," *Science* **281**, 2016-2018 (1998) [[doi:10.1126/science.281.5385.2016](https://doi.org/10.1126/science.281.5385.2016)].
- [35] C.-J. Wang, L. Y. Lin, and B. A. Parviz, "Modeling and simulation for a nano-photonic quantum dot waveguide fabricated by DNA-directed self-assembly," *IEEE J. Quantum Electron.* **11**, 500-509 (2005) [[doi:10.1109/JSTQE.2005.845616](https://doi.org/10.1109/JSTQE.2005.845616)].
- [36] C.-J. Wang, L. Y. Lin, and B. A. Parviz, "100-nm quantum dot waveguides by two-layer self-assembly," *Proc. 18th Annu. Mtg. IEEE LEOS*, 194-195 (2005) [[doi:10.1109/LEOS.2005.1547936](https://doi.org/10.1109/LEOS.2005.1547936)].
- [37] L. Huang, C.-J. Wang, and L. Y. Lin, "A comparison of crosstalk effects between colloidal quantum dot waveguides and conventional waveguides," *Opt. Lett.* **32**, 235-237 (2007) [[doi:10.1364/OL.32.000235](https://doi.org/10.1364/OL.32.000235)].
- [38] C.-J. Wang, L. Huang, B. A. Parviz, and L. Y. Lin, "Sub-diffraction photon guidance by quantum dot cascades," *Nano Lett.* **6**, 2549-2553 (2006) [[doi:10.1021/nl061958g](https://doi.org/10.1021/nl061958g)].
- [39] C.-J. Wang and L. Y. Lin, "Nanoscale waveguiding methods," *Nanoscale Res. Lett.* **2**, 219-229 (2007) [[doi:10.1007/s11671-007-9056-6](https://doi.org/10.1007/s11671-007-9056-6)].
- [40] C. J. Wang, B. A. Parviz and L. Y. Lin, "Two dimensional array self-assembled quantum dot sub-diffraction waveguides with low loss and low crosstalk," *Nanotechnology* **19**(23), 295201 (2008) [[doi:10.1088/0957-4484/19/29/295201](https://doi.org/10.1088/0957-4484/19/29/295201)].
- [41] J. F. Wang, M. S. Gudiksen, X. F. Duan, Y. Cui, and C. M. Lieber, "Highly polarized photoluminescence and photodetection from single indium phosphide nanowires," *Science* **293**, 1455-1457 (2001) [[doi:10.1126/science.1062340](https://doi.org/10.1126/science.1062340)].
- [42] O. Hayden, R. Agrawal, and C. M. Lieber, "Nanoscale avalanche photodiodes for highly sensitive and spatially resolved photon detection," *Nature Mater.* **5**, 352-356 (2006) [[doi:10.1038/nmat1635](https://doi.org/10.1038/nmat1635)].
- [43] M. Freitag, Y. Martin, J. A. Misewich, R. Martel, and P. H. Avouris, "Photoconductivity of single carbon nanotubes," *Nano Lett.* **3**, 1067-1071 (2003) [[doi:10.1021/nl034313e](https://doi.org/10.1021/nl034313e)].
- [44] O. Astafiev and S. Komiyama, "Single-photon detection with quantum dots in the far-infrared/submillimeter-wave range," in *Electron Transport in Quantum Dots*, 1st ed., J. P. Bird, Ed., pp. 363-396, Kluwer Academic Press, Boston (2003).
- [45] O. Astafiev, S. Komiyama, T. Kutsuwa, V. Antonov, Y. Kawaguchi, and K. Kirakawa, "Single-photon detector in the microwave range," *Appl. Phys. Lett.* **80**, 4250-4252 (2002) [[doi:10.1063/1.1482787](https://doi.org/10.1063/1.1482787)].
- [46] J. Alda, J. M. Rico-Garcia, J. M. Lopez-Alonso, and G. Boreman, "Optical antennas for nano-photonic applications," *Nanotechnology* **16**, S230-S234 (2005) [[doi:10.1088/0957-4484/16/5/017](https://doi.org/10.1088/0957-4484/16/5/017)].
- [47] K. T. Posani, V. Tripathi, S. Annamalai, N. R. Weisse-Bernstein, S. Krishna, R. Perahia, O. Crisafulli, and O. J. Painter, "Nanoscale quantum dot infrared sensors with photonic crystal cavity," *Appl. Phys. Lett.* **88**, 151104 (2006) [[doi:10.1063/1.2194167](https://doi.org/10.1063/1.2194167)].
- [48] R. D. Schaller, M. Sykora, S. Jeong, and V. I. Klimov, "High-efficiency carrier multiplication and ultrafast charge separation in semiconductor nanocrystals

- studied via time-resolved photoluminescence," *J. Phys. Chem. B* **110**, 25332-25338 (2006) [[doi:10.1021/jp065282p](https://doi.org/10.1021/jp065282p)].
- [49] R. D. Schaller, M. Sykora, J. M. Pietryga, and V. I. Klimov, "Seven excitons at a cost of one: Redefining the limits for conversion efficiency of photons into charge carriers," *Nano Lett.* **6**, 424-429 (2006) [[doi:10.1021/nl052276g](https://doi.org/10.1021/nl052276g)].
- [50] M. C. Hegg and L. Y. Lin, "Near-field photodetection with high spatial resolution by nanocrystal quantum dots," *Opt. Exp.* **15**, 17163-17170 (2007) [[doi:10.1364/OE.15.017163](https://doi.org/10.1364/OE.15.017163)].
- [51] L. Huang, M. C. Hegg, C.-J. Wang, and L. Y. Lin, "Fabrication of a nanophotonic waveguide and photodetector integrated device," *Micro Nano Lett.* **2**, 103-106 (2007) [[doi:10.1049/mnl:20070053](https://doi.org/10.1049/mnl:20070053)].
- [52] W. Hu, K. Sarveswaran, M. Lieberman, and G. H. Bernstein, "High-resolution electron beam lithography and DNA nano-patterning for molecular QCA," *IEEE Trans. Nanotech.* **4**, 312-316 (2005) [[doi:10.1109/TNANO.2005.847034](https://doi.org/10.1109/TNANO.2005.847034)].
- [53] L. M. Demers, D. S. Singer, S.-J. Park, Z. Li, S.-W. Chung, and C. A. Mirkin, "Direct patterning of modified oligonucleotides on metals and insulators by dip-pen nanolithography," *Science* **296**, 1836-1838 (2002) [[doi:10.1126/science.1071480](https://doi.org/10.1126/science.1071480)].
- [54] United Chemical Technologies, "Using Silanes as Adhesion Promoters." <http://www.unitedchem.com>.
- [55] W. Hu, K. Sarveswaran, M. Lieberman, and G. H. Bernstein, "High-resolution electron beam lithography and DNA nano-patterning for molecular QCA," *IEEE Trans. Nanotech.* **4**, 312-316 (2005) [[doi:10.1109/TNANO.2005.847034](https://doi.org/10.1109/TNANO.2005.847034)].
- [56] F. Kusunoki, T. Yotsuya, J. Takahara, and T. Kobayashi, "Propagation properties of guided waves in index-guided two-dimensional optical waveguides," *Appl. Phys. Lett.* **86**, 21110 (2005) [[doi:10.1063/1.1935034](https://doi.org/10.1063/1.1935034)].
- [57] D. Ginger and N. Greenham, "Electrical properties of semiconductor nanocrystals," in *Semiconductor and Metal Nanocrystals: Synthesis and Electronic and Optical Properties*, V. I. Klimov, Ed, Marcel Dekker, New York (2004).
- [58] H. C. Liu and G. C. Aers, "Resonant tunneling through one-dimensional, two-dimensional, and 3-dimensionally confined quantum wells," *J. Appl. Phys.* **65**, 4908-4914 (1989) [[doi:10.1063/1.343427](https://doi.org/10.1063/1.343427)].
- [59] A. K. Mahapatro, S. Ghosh, and D. B. Janes, "Nanometer scale electrode separation (Nanogap) using electromigration at room temperature," *IEEE Trans. Nanotech.* **5**, 232-236 (2006) [[doi:10.1109/TNANO.2006.874053](https://doi.org/10.1109/TNANO.2006.874053)].